Wireless Cooperative Synchronization of Coherent UWB MIMO Radar

Sunwoo Kong, *Student Member, IEEE*, Sungeun Lee, *Student Member, IEEE*, Choul-Young Kim, *Associate Member, IEEE*, and Songcheol Hong, *Member, IEEE*

***Abstract*—We present a synchronization method and coherent ultra-wideband transceivers for a widely separated multiple-input multiple-output (MIMO) radar. Synchronization is essential for MIMO operation, but a spatially spread radar array is not a good structure for it. A wireless cooperative synchronization method is based on coherency of pulse signals and highly accurate delay estimation and they are implemented through a coherent pulse generator and a fine delay-based receiver. Distance measurements of a radar transceiver (TRX) show that the maximum mean error is 4 mm for the target in a range of 0.2 m–8.0 m. Synchronization measurements of two radar TRXs show that the maximum mean error of the asynchronous time difference is 11 ps for the target in a range of 0.25–8.0 m. 2-D images for multiple targets and fluctuational radar cross sections are achieved with the proposed synchronization method under MIMO operation.**

***Index Terms*—CMOS, multiple-input multiple-output (MIMO), radar, synchronization, ultra-wideband (UWB).**

I. Introduction

RADAR ARRAYS are now being widely used for location applications. In general, there are two types of arrays according to how far the radar antennas are spaced: radar arrays with colocated antennas scan targets with a sharp beam and find the locations of targets [1]–[4] and radar arrays with widely separated antennas find target locations by using trilateration [5]–[7].

The multiple-input multiple-output (MIMO) radar jointly processes multiple signals from multiple radar transceivers (TRXs) to acquire spatial diversity gain, improved location estimation, and an increased range of detection. Synchronization among the radar TRXs is very important for the MIMO operation in both types of radar arrays [8], [9].

Contrary to radar arrays with colocated antennas, where multiple TRXs are integrated in a chip, radar arrays with widely separated antennas have difficulties in synchronization because the TRXs are spread in space. In addition, distances among TRXs need to be comparable to target distance to get enough diversity gain and cross-range resolution [5]–[7]. A wireless cooperative synchronization method has an important role in spatially spread radars. In the case of frequency modulated continuous wave (FMCW) radars, wireless synchronization methods have been studied in the frequency domain for active target detection [10]–[12]. Since an ultra-wideband (UWB) pulsed radar is based on a time-domain analysis, the synchronization error has significant effects on its operation. Coherent operation is necessary for the wireless cooperation synchronization method to reduce this error. Coherent pulse generation and fine delay-based correlation are required for cooperative operation and accurate estimation of the traveling time of a pulse signal, respectively. A typical pulsed radar operates noncoherently [13]–[16] and it cannot use phase information for synchronization. A proposed UWB pulsed radar uses coherent pulses with a fine delay-based correlator to synchronize among the radars for MIMO operation.

A MIMO radar needs a large number of TRXs since the use of many TRXs improves the radar performance [9], [17]. The power consumption in multiple radar TRXs becomes a very important issue. A current-reusing low-noise mixer and pulsed oscillator contribute to reduction of the total power consumption. The delay controller in the UWB radar TRX is a digital circuit, which can be easily integrated in a single chip with the RF front-ends using CMOS technology.

Here, we propose a wireless synchronization method and a low-power UWB MIMO radar that is composed of a coherent pulse generator and a fine delay-based correlator.

II. Proposed UWB MIMO Radar

A block diagram of the UWB MIMO radar is depicted in Fig. 1. Multiple UWB radar TRXs are used to form the UWB MIMO radar. The relative location of each TRX with an antenna does not have a certain relation, contrary to the case of radar arrays with colocated antennas. The TRX estimates the distance of a target by controlling the pulse delay [18]. After a pulse signal is transmitted to targets, the delayed local pulse signal is fed into the mixer of the receiver and correlated with an echo signal to measure traveling time of the pulse signal relative to transmit time. A train of pulses appears at the output of the mixer when the controlled delay and the round-trip time of the pulse signal are the same.

The MIMO radar transmits multiple pulses from multiple transmitters and jointly processes echo signals received at multiple receivers. The MIMO operation improves the spatial diversity gain, which brings robustness to fluctuation of the radar

Manuscript received August 06, 2013; revised October 31, 2013; accepted October 31, 2013. Date of publication November 22, 2013; date of current version January 06, 2014. This work was supported by the Korea Government (MEST) under National Research Foundation of Korea (NRF) Grant 2009-0080805.

S. Kong, S. Lee, and S. Hong are with the School of Electrical Engineering and Computer Science, Department of Electrical Engineering and Computer Science, Korea Advanced Institute of Science and Technology (KAIST), Daejeon 305-701, Korea (e-mail: throckmorton@kaist.ac.kr; pick42@kaist.ac.kr; schong@ee.kaist.ac.kr).

C.-Y. Kim is with the Electronics Engineering Department, Chungnam National University, Daejeon 305-764, Korea (e-mail: cykim@cnu.ac.kr).

Color versions of one or more of the figures in this paper are available online at http://ieeexplore.ieee.org.

Digital Object Identifier 10.1109/TMTT.2013.2291541

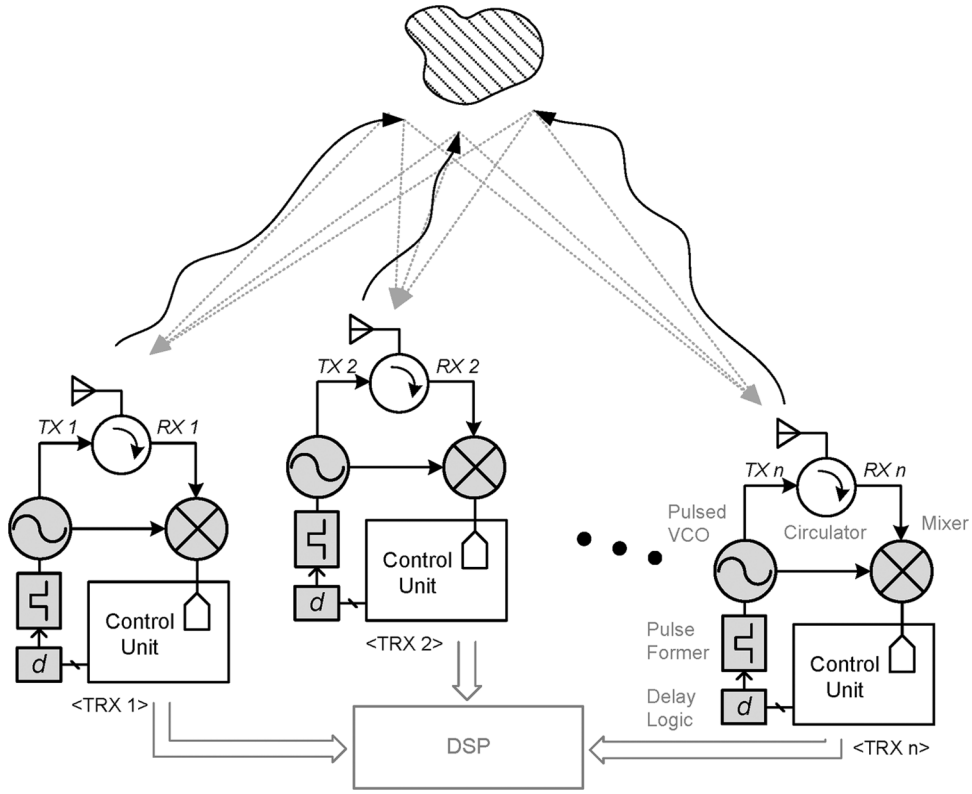

Fig. 1. UWB MIMO radar array.

cross section (RCS), and tolerance to multiple targets [9]. In Fig. 1, TRX 1 transmits a pulse signal, and receives echo signals from not only TRX 1, but also TRX 2, TRX 3, and so on, and the others fulfill the same role as TRX 1. Since TRXs are spread in space, it is difficult to process pulse signals of other TRXs. A delay circuit should be placed between TRX 1 and 2 for MIMO operation to get the same accuracy of estimating the traveling time of a pulse from TRX 1 to TRX 2 as the single radar operation. In case of TRX 1, 2, and 3, a network of six delay circuits are necessary. A network of the delay circuits becomes complex as the number of radar TRXs increases for MIMO operation. This complex delay network for MIMO operation, which exists in the central unit, also lowers the flexibility of radar arrays because every connection line of delay circuits cannot be immediately calibrated according to flexible positions of radar TRXs.

We propose a wireless cooperative synchronization method and coherent UWB radar to solve these problems. A transmitter and a receiver are integrated in a chip and used as an element of a MIMO radar array. The TRX is a standalone UWB radar and it provides flexible formation of a radar array. Each TRX knows only the transmit time of its own signal. The MIMO operation needs to know the transmit times of the other TRXs using synchronization. TRX 1 and 2 swap their pulse signals for synchronization. TRX 1 receives and processes the echo signals from TRX 2, and vice versa. The central processor can find the time difference of the asynchronous TRXs by using the digital values of the measured time delays of the swapped pulse signals. Coherent processing is required for this wireless cooperative synchronization and a UWB radar TRX with a coherent pulse generator and a fine delay-based correlator is proposed for the synchronization. Sections III and IV describe the coherent UWB radar TRX and the wireless cooperative synchronization method, respectively.

III. Proposed Coherent UWB Radar TRX

A. Signal Model

The UWB radar TRX receives the pulse signal that is transmitted from the TRX and reflected by the target. The round-trip time of the pulse signal is estimated by correlation with the time-delayed local pulse signal generated by a delay circuit. The UWB transmit signal from TRX n can be described as

$$S_{T,n}(t) = \sum_{k=-\infty}^{\infty} A_n h(t - kT_P) \cos[\omega t + \varphi_n(t)] \quad (1)$$

$$h(t) = \begin{cases} 1, & 0 < t < T_{pw} \\ 0.5, & t = 0, t = T_{pw} \\ 0, & \text{otherwise} \end{cases} \quad (2)$$

where A_n, T_P, ω, and $\varphi_n(t)$ are the amplitude, the pulse repetition interval (PRI), the carrier frequency, and the carrier phase of the transmit signal of the TRX n, respectively. The pulsewidth of the UWB signal is T_{pw}, which defines the range resolution of the UWB radar TRX. The received echo signal of the TRX n is

$$S_{R,n}(t) = \sum_{k=-\infty}^{\infty} \alpha A_n h\left(t - \frac{2R}{c} - kT_P\right) \times \cos\left[\omega\left(t - \frac{2R}{c}\right) + \varphi_n'(t)\right] \quad (3)$$

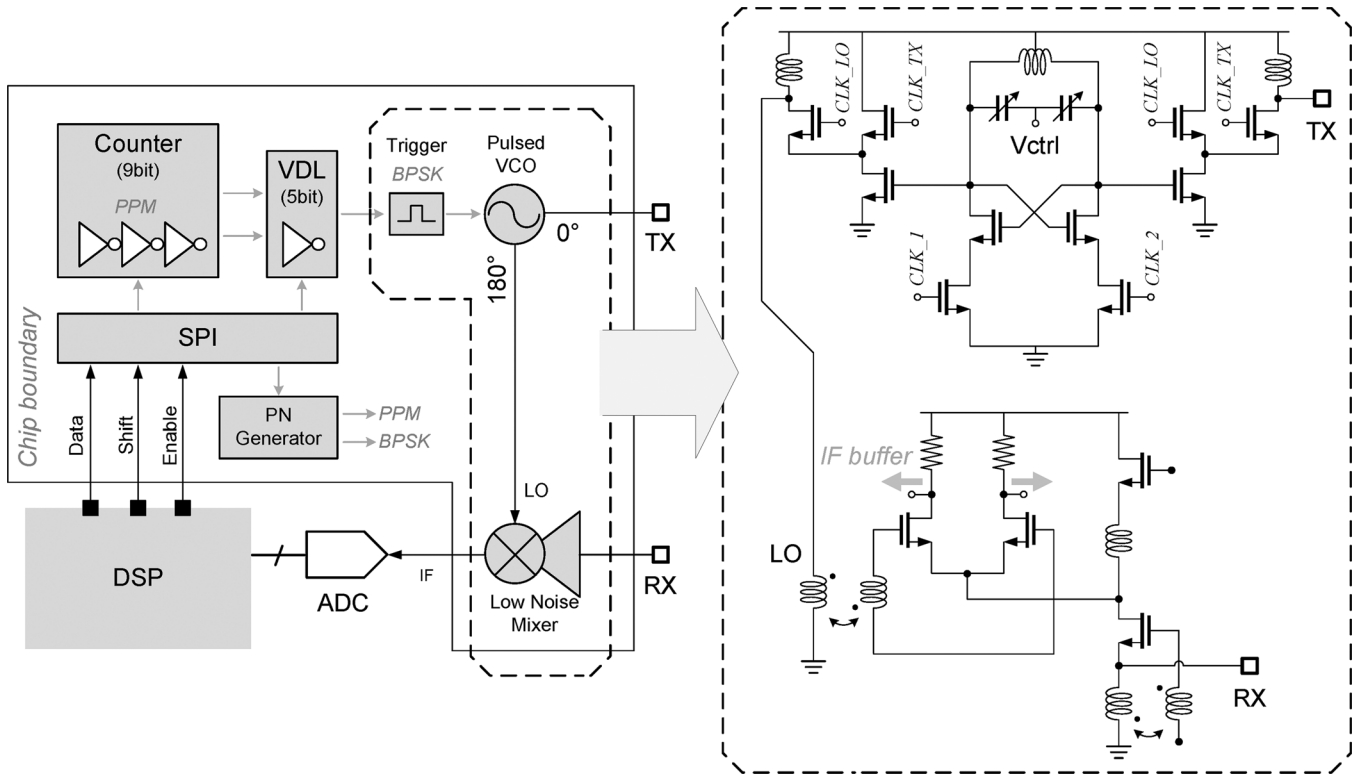

Fig. 2. Block diagram of the UWB radar TRX.

where R is the distance between TRX n and the target, c is the free-space propagation velocity of radio waves, and $\varphi'_n(t)$ is the carrier phase of the received echo signal of the TRX n. The received signal consists of the transmit signal, which is attenuated by α and delayed by $2R/c$. The latter is the round-trip time between the TRX n and the target. To estimate the distance R, the UWB radar TRX checks the correlation of the received echo signal with the time-delayed local pulse signal. The time-delayed local pulse signal is shown as

$$S_{\mathrm{LO},n}(t) = \sum_{k=-\infty}^{\infty} A_n h(t - T_d - kT_P) \times \cos[\omega(t - T_d) + \varphi''_n(t)] \quad (4)$$

where T_d is the controlled delay time and $\varphi''_n(t)$ is the carrier phase of time-delayed local pulse signal of the TRX n. The received echo signal and the time-delayed local pulse signal are correlated by a mixer. A train of baseband pulses appears at the output of the mixer when T_d approaches $(2R)/(c)$. The baseband output signal after low-pass filtering is described as

$$S_{\mathrm{IF},n}(t) = \sum_{k=-\infty}^{\infty} \frac{\alpha A_n^2}{2} h(t - T_d - kT_P) h\left(t - \frac{2R}{c} - kT_P\right) \cdot \cos\left[\omega\left(T_d - \frac{2R}{c}\right) + \varphi'_n(t) - \varphi''_n(t)\right]. \quad (5)$$

The second and third factors on the right-hand side of (5) show the overlapped envelope of the pulse, and the fourth factor describes the phase relation between the received echo signal and the time-delayed local pulse signal. Since noncoherent signals make an irregular phase relation in the pulse train, it is necessary to consider only the envelope of the pulse signal. On the other hand, when coherent signals can be used, the phase information of the carrier can be acquired because the phases $\varphi'_n(t)$ and $\varphi''_n(t)$ are not changed over repetitive pulses. The coherent processing has better accuracy than the noncoherent processing due to the phase information.

B. Coherent Pulses and Correlation

A block diagram of the proposed UWB radar TRX is shown in Fig. 2 [18]. The TRX consists of a pulsed oscillator, a current-reusing low noise mixer, and a digital delay circuit. The UWB radar TRX scans the range around the targets by controlling the delay. The delay is defined by the relative time difference between the transmit pulse signal and the local pulse signal. Two timing signals, of which the interval is controlled, trigger the pulsed VCO. The timing signals, CLK_TX and CLK_LO in Fig. 2, transmit a TX signal and a delayed LO signal, respectively. The counter makes a coarse delay, and the vernier delay logic (VDL) makes a fine delay to find phase information. Pulse position modulation (PPM) and bi-phase shift keying (BPSK) modulation are applied for the spread spectrum and simultaneous operation of multiple radars.

The coherent correlation is described in Fig. 3. TX is the transmit pulse signal, which makes a round-trip between the TRX and the target during t_{round}. The delay circuit allows estimation of this t_{round} by correlating the RX and LO. The RX, LO, and IF are the received signal reflected from the target, the delayed local pulse signal fed into the correlator, and the correlated output signal, respectively. The very fine delay, which must have a time step of less than the carrier period, causes periodic amplitude fluctuation of the correlated output signal with

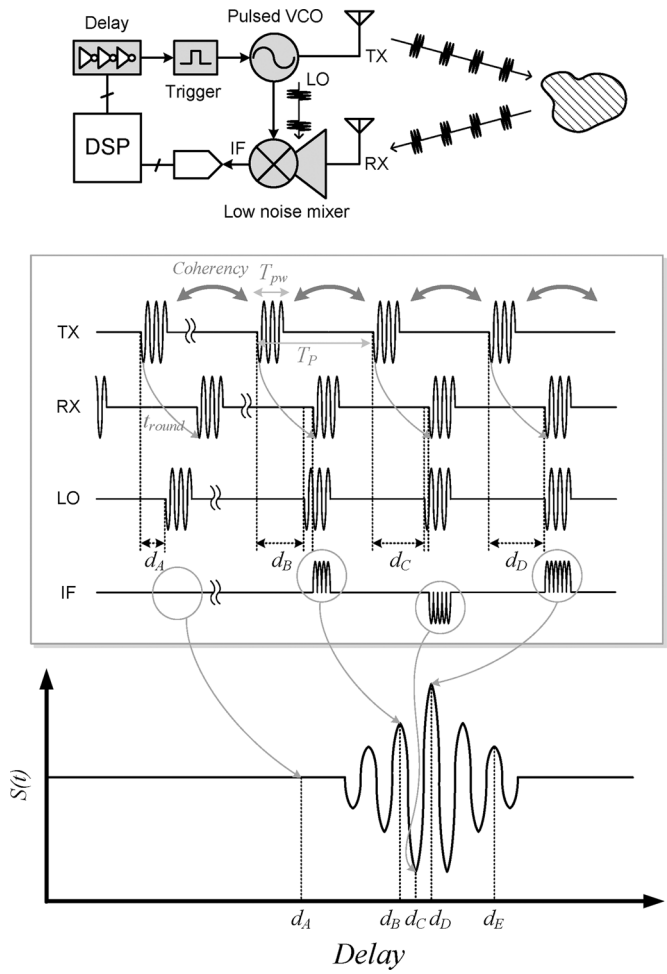

Fig. 3. Coherent operation of the UWB radar TRX.

respect to the phase difference between the received signal and the delay-swept local signal.

The range scan of the UWB radar TRX is not completed during a cycle, as depicted in Fig. 3. Since the RX pulse signal is repetitive, the delayed time of the LO is increased stepwise and the RX pulses are correlated over multiple delayed LO pulses that complete the PRI. The correlated signals are integrated at a certain delay to increase the signal-to-noise ratio (SNR) [19]. The UWB radar TRX uses the equivalent-time (ET) sampling principle as in a digital sampling oscilloscope. The ET operation relaxes the high-speed operation requirement of a delay circuit, as well as an analog-to-digital converter. Although a parallel receiver can provide a solution to have high-speed operation, it is not suitable for a low-power low-cost system for a multiple radar system.

Phase information is required for not only improved range accuracy of a radar operation, but also wireless synchronization. There are two essential factors for coherent correlation. First, the repetitive pulse signals must be coherent. If the coherency is not assured, the RX and the LO may have a random phase relation, and the IF cannot give any phase information, as can be seen in (5). The pulsed oscillator maintains a uniform phase of transmitted pulses by turning on a differential current source at slightly different timings (CLK_1 & CLK_2) when it starts to oscillate [20]. A continuous oscillator and a pulse-shaping switch have difficulties to make coherent pulses, which are typically used for noncoherent processing [13]–[16].

Second, the delay step should be very fine. In general, a very fine delay step is not needed. The delay step of the pulsewidth is usually short enough to scan the whole target range. However, a delay step shorter than the period of a carrier provides the phase information. Here, the period of a 26-GHz carrier is 38.5 ps and the minimum delay step is 5.5 ps. Approximately seven steps are required to scan the period. In Fig. 3, the delay d_A shows no targets. The delay d_D indicates the maximum overlap area and the in-phase between the RX and the LO signals, which corresponds to the exact target distance. The delays of d_B, d_C, and d_E, respectively, represent phases of -360°, -180°, and 720° with respect to the maximum overlap and in-phase point.

C. Low Power Consumption

In general, the performance measures of a MIMO radar such as diversity, multiple target detection, and operating cross-range are improved as the number of TRXs increases at the cost of power consumption [9], [17]. The TRX, as a basic element of the MIMO radar, should consume low power for MIMO operation. Here, a pulsed oscillator and a current-reusing low-noise mixer are applied to the TRXs to reduce power consumption.

The UWB TRX uses pulse signals to detect targets, and consequently the oscillator of the TRX does not have to be always turned on. A conventional pulse generator makes a continuous-wave signal and shapes it into pulses using a switch [13]–[16]. However, a pulsed oscillator makes pulse signals by turning on and off the oscillator itself [20]. The conventional pulse generator consumes power continuously, but the pulsed oscillator consumes power only when it is turned on. The duty cycle of pulse signals is extremely low, and as a result, the power consumption is also kept very low. For example, a pulsed oscillator with 4-MHz pulse repetition frequency (PRF) and 500-ps pulsewidth has only a 0.2% duty cycle. This corresponds with 500 times lower power consumption than that of a continuous oscillator.

A conventional low-noise amplifier (LNA) needs high power consumption to simultaneously obtain wide bandwidth, high gain, and a low noise figure, because multiple stages are necessary to realize these functions. The current-reusing low-noise mixer avoids multiple stages of RF amplification at the cost of high noise and low conversion gain. To improve the conversion gain and the noise figure, transformer g_m-boosting and bleeding path g_m-boosting techniques, which do not involve additional power consumption, are applied [21].

D. Digitally Controlled Delay

The coherent correlation takes a long time to scan the target range because of the very short delay step. This becomes severe with the use of the ET sampling operation. A digital delay circuit that can randomly control the delay value relaxes this problem. A search algorithm can be adopted through this digital delay to find an exact delay value for a target distance, and this is expected to drastically reduce the scan time.

The ET correlation takes a PRI per a step of the delay. It takes a long time to cover all of the target range. Furthermore,

integration of pulses is needed to improve SNR. The time to scan the target range is shown as

$$T_{\text{scan}} = \frac{n(2R/c)^2}{d_{\min}} \tag{6}$$

where R, n, and $d_{\min}$ are the target range, the integration number, and the minimum delay step, respectively. The scan time is equal to 808 ms, when $R = 10$ m, $n = 1000$, and $d_{\min} = 5.5$ ps. This is a long refresh time for a fast moving target.

The digital delay provides a coarse scan mode. It is not necessary to scan the whole target range finely to detect a target, as described above. The coarse scan mode finds the approximate distance of a target and then the fine scan mode checks the exact range around it. The fine and coarse scan modes use 5.5- and 500-ps delay steps, respectively. Since the pulsewidth is 500 ps, a 500-ps coarse delay step can be used to scan the target range without exception. Each coarse scan is performed by using two repeated pulses with a small delay interval, which corresponds to a 90° phase difference. This method with two orthogonal pulses obviates the use of in-phase and quadrature (I/Q) signals to avoid a null point problem. The total scanning time can thus be reduced by a factor of 11/500 with the coarse scan mode compared to that only with the fine scan mode.

The integration number can be controlled according to the target distance. Since the far-field target reflects a low power signal, a large number of integrations is required to improve the SNR, but the near-field target needs a small number of integrations. Since the received power is increased in proportion to $1/R^4$, the integration number is reduced by as much as 1/5th when the adaptive integration number is applied according to the target distance. The total reduced time to scan the target range is shown as

$$T_{\text{scan}} = \frac{n(2R/c)^2}{227 \cdot d_{\min}}. \tag{7}$$

When $R = 10$ m, $n = 1000$, and $d_{\min} = 5.5$ ps, T_{scan} is approximately 3.6 ms. The coarse scan mode and the adaptive integration from the digital delay decrease the scan time and improve the performance of tracking a target.

IV. Wireless Cooperative Synchronization of UWB MIMO Radar Operation

A. Signal Model

A TRX of the UWB MIMO radar receives the pulse signals from not only itself, but also others. The transmit pulse signal of TRX n, which is expected to be received by TRX m, is described as

$$S_{T,mn}(t) = \sum_{k=-\infty}^{\infty} A_n h(t - \delta_{mn} - kT_P) \times \cos[\omega(t - \delta_{mn}) + \varphi_n(t)] \tag{8}$$

where δ_{mn} is the time difference due to asynchronous operation of TRX m and n. The UWB radar TRXs are not synchronized, and hence, a random value of δ_{mn} must be introduced.

The echo signal received by TRX m, which is transmitted from TRX n and reflected by the target, is given as

$$S_{R,mn}(t) = \sum_{k=-\infty}^{\infty} \alpha A_n h\left(t - \frac{R_m + R_n}{c} - \delta_{mn} - kT_P\right) \cdot \cos\left[\omega\left(t - \frac{R_m + R_n}{c} - \delta_{mn}\right) + \varphi'_n(t)\right] \tag{9}$$

where R_m and R_n are the distances between the target and the TRX m and n, respectively. The time-delayed local signal of the TRX m is described as

$$S_{\text{LO},m}(t) = \sum_{k=-\infty}^{\infty} A_m h(t - T_d - kT_P) \times \cos[\omega(t - T_d) + \varphi_m(t)] \tag{10}$$

and the baseband output signal is expressed as

$$\begin{aligned} S_{\text{IF},m}(t) &= \sum_{k=-\infty}^{\infty} \frac{\alpha A_m A_n}{2} \\ &\quad \cdot h(t - T_d - kT_P) h\left(t - \frac{R_m + R_n}{c} - \delta_{mn} - kT_P\right) \\ &\quad \cdot \cos\left[\omega\left(T_d - \frac{R_m + R_n}{c} - \delta_{mn}\right) + \varphi'_n(t) - \varphi_m(t)\right]. \end{aligned} \tag{11}$$

An unknown time difference δ_{mn} makes it difficult to estimate $R_m + R_n$. The time of $(R_m + R_n)/(c) + \delta_{mn}$ can be found by scanning the delay in TRX m because the reference time of the delay is the transmit time of TRX m. Since the phases of TRX n and m, $\varphi'_n(t)$ and $\varphi_m(t)$, are kept constant, coherent processing of the synchronization is possible.

B. Wireless Cooperative Synchronization Method

A wireless cooperative synchronization method is used to find the asynchronous time difference δ_{mn}. This method is applied to a pair of TRXs among multiple TRXs for MIMO operation to find the time difference between them. The synchronization process is described in Fig. 4. TRX 1 and 2 swap their pulse signals. TRX 1 receives and processes an echo signal from TRX 2, and vice versa.

The asynchronous time difference between TRX 1 and 2 is δ_{21}, which is larger than zero and smaller than T_P. Four cases of ambiguities of estimating δ_{21} are shown according to the relation of $\delta_{21}, T_p, t_{d12}$, and t_{d21} in Fig. 5. For simplification, self-correlations d_{11} and d_{22} are not marked. The traveling time of pulses from TRX 1, through the target to TRX 2, and *vice versa* are t_{d21} and t_{d12}, respectively, and these are the same $(t_d = t_{d21} = t_{d12})$ because they have the same traveling length. The controlled delays of TRX 1 and 2 are d_{12} and d_{21}, respectively. From Fig. 5, the measured delays of TRX 1 and 2 are described as

$$\begin{cases} d_{12} = t_{d12} - (T_P - \delta_{21}) \\ d_{21} = t_{d21} - \delta_{21} \end{cases} \tag{12}$$

$$\begin{cases} d_{12} = t_{d12} + \delta_{21} \\ d_{21} = t_{d21} - \delta_{21} \end{cases} \tag{13}$$

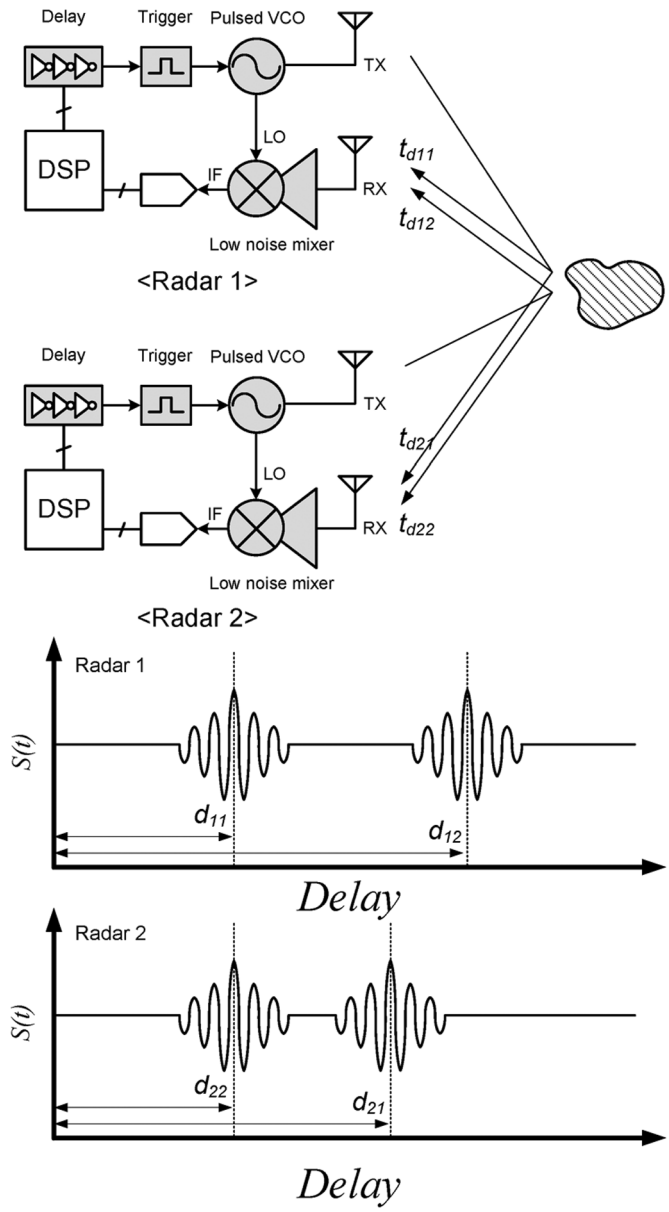

Fig. 4. Synchronization process.

$$\begin{cases} d_{12} = t_{d12} + \delta_{21} \\ d_{21} = t_{d21} + (T_P - \delta_{21}) \end{cases} \tag{14}$$

$$\begin{cases} d_{12} = t_{d12} - (T_P - \delta_{21}) \\ d_{21} = t_{d21} + (T_P - \delta_{21}) \end{cases} \tag{15}$$

according to Fig. 5(a)–(d), respectively. The asynchronous time difference is drawn from these relations, and described as

$$\delta_{21} = \begin{cases} \dfrac{d_{12} - d_{21} + T_P}{2} & (16) \\ \dfrac{d_{12} - d_{21}}{2} & (17) \\ \dfrac{d_{12} - d_{21} + T_P}{2} & (18) \\ \dfrac{d_{12} - d_{21} + 2T_P}{2} & (19) \end{cases}$$

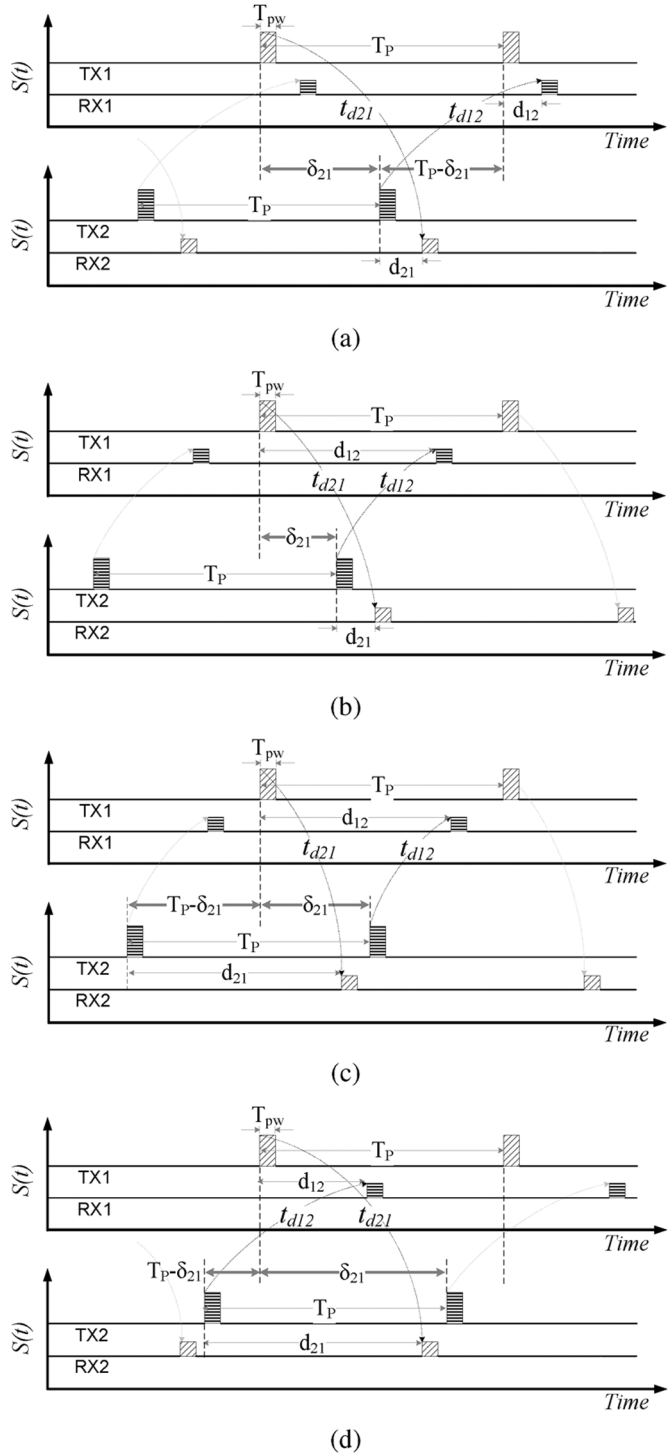

Fig. 5. Timing diagrams of the transmitted and received signals between TRX 1 and TRX 2 when: (a) $\delta_{21} < t_d$ and $\delta_{21} + t_d > T_P$, (b) $\delta_{21} < t_d$ and $\delta_{21} + t_d < T_P$, (c) $\delta_{21} > t_d$ and $\delta_{21} + t_d < T_P$, and (d) $\delta_{21} > t_d$ and $\delta_{21} + t_d > T_P$.

when $\delta_{21} < t_d$ and $\delta_{21} + t_d > T_P$, $\delta_{21} < t_d$ and $\delta_{21} + t_d < T_P$, $\delta_{21} < t_d$ and $\delta_{21} + t_d < T_P$, and $\delta_{21} > t_d$ and $\delta_{21} + t_d > T_P$, respectively.

Two conditions are proposed to solve the ambiguity problem of estimating δ_{21}. We should select a proper case by the measured values of d_{11}, d_{22}, d_{12}, and d_{21}. In Table I, factors of conditions for the ambiguity problem are shown. First, $d_{11}+d_{22}$ and

TABLE I
FACTORS OF CONDITIONS FOR THE AMBIGUITY PROBLEM OF ESTIMATING δ_{21}

Cases	$d_{11}+d_{22}$	$d_{12}+d_{21}$	$d_{12}-d_{21}$
Equation (16)	$2t_d$	$2t_d-T_P$	$-T_P+2\delta_{21}$
Equation (17)	$2t_d$	$2t_d$	$2\delta_{21}$
Equation (18)	$2t_d$	$2t_d+T_P$	$-T_P+2\delta_{21}$
Equation (19)	$2t_d$	$2t_d$	$-2(T_P-\delta_{21})$

$d_{12}+d_{21}$ are compared. The former has a value of $2t_d$ in every case, but the latter has values of $2t_d-T_P$, $2t_d$, $2t_d+T_P$, and $2t_d$ according to (12)–(15), respectively. Equations (16) and (18) are the cases of $d_{11}+d_{22} > d_{12}+d_{21}$ and $d_{11}+d_{22} < d_{12}+d_{21}$, respectively. Therefore, cases of (16) and (18) can be known. However, another condition is required for (17) and (19) because both of them are the case of $d_{11}+d_{22} = d_{12}+d_{21}$. Second, d_{12} and d_{21} are compared. In the case of (13), $d_{12}-d_{21}$ is larger than zero because $d_{12}-d_{21}$ is equal to $2\delta_{21}$, whereas, in the case of (15), $d_{12}-d_{21}$ is smaller than zero because $d_{12}-d_{21}$ is equal to $-2(T_P-\delta_{21})$. Equations (17) and (19) are the cases of $d_{12}-d_{21}>0$ and $d_{12}-d_{21}<0$, respectively. The ambiguities of estimating δ_{21} are solved by considering these conditions.

The phase information from the very fine delay, which has a smaller delay step than the period of the carrier, provides highly accurate estimation of the asynchronous time difference. An I/Q receiver can also provide phase information, which is a relative local delay within a period of the carrier and therefore it is generally used in continuous waveform radar systems. In pulsed radar systems, it requires the delay information outside of a period of carrier to know pulse envelopes. The coherent fine delay-based radar acquires phase information, which is the fourth factor of (11), and an overlapped area of pulse envelopes, which is a product of the second and third factors of (11). The estimation accuracy of δ_{21} affects all of the measurement results after the calibration. Since the UWB radar TRX calibrates the asynchronous time difference with a 5.5-ps delay step, the UWB radar TRX has a potential range error of only 0.825 mm.

V. MEASUREMENT RESULTS

A. Range Estimation and Synchronization

The UWB MIMO radar is composed of multiple UWB radar TRXs. Photographs of the chip and the TRX module are presented in Figs. 6 and 7, respectively. The chip is implemented in a 0.13-μm CMOS process and its size is 1.07×1.28 mm^2. The total power consumption of the core circuit is 6.89 mA with a supply voltage of 1.5 V. A high-frequency material (RO3003) board is stacked on an FR4 board to use a branch line coupler for a circulator. Two commercially available chips are used for measurement. The input of the digital circuit is fed from the buffer gate chip (74ALVC125) to protect the small input transistors of the digital circuit. The differential output of the receiver is converted to a single-ended output by a transformer chip (Mini-Circuit ADT2-1T-1P) for impedance matching.

The measurement setup for the UWB radar TRX is shown in Fig. 8. The target is a metal plate with a size of 30 cm $\times$ 30 cm, and it is moved back and forth along a rail. The delay of the TRX is controlled by a PC. The output signal is acquired by an analog-to-digital converter, and an oscilloscope (LeCroy SDA6020) is used here. The UWB radar module is driven by AA batteries and operates with a horn antenna (Quinstar Tech. QWH-KCRS00).

The measured raw data is described in Fig. 9(a). Pulse A is the correlation output of a TX pulse and its leakage signal. The leakage is mostly due to insufficient isolation of the branch line coupler at the output. However, this leakage does not affect the radar operation because of the time-gated feature of pulsed radars. It instead becomes an indicator that describes the time of transmitting a pulse signal. The time from A to A* is the PRI. The time from A to B is the controlled delay because pulse B is the correlation output of a received echo pulse and a delayed-local pulse. In Fig. 9(b), an enlarged figure of pulse B is shown with varying VDL. The target is 0.5 m away from the radar TRX. The fluctuation of pulse B shows the phase and

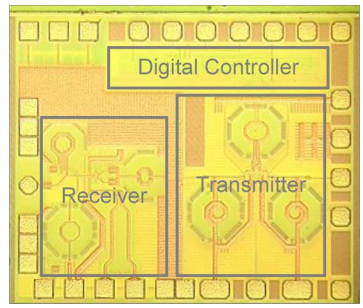

Fig. 6. Microphotograph of the UWB radar TRX IC. The chip size is 1.07×1.28 mm^2.

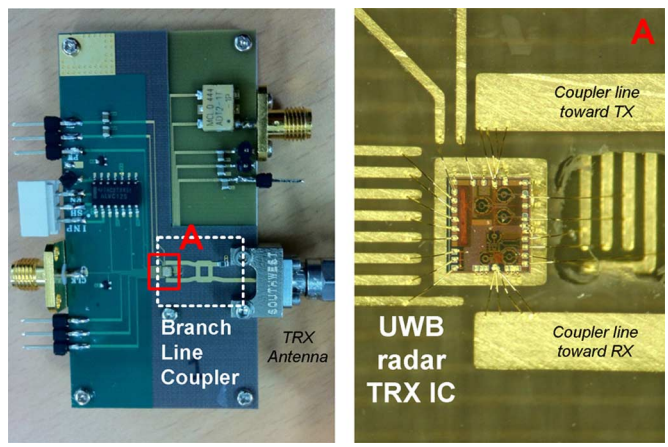

Fig. 7. Photograph of the UWB radar TRX module. A branch line coupler is used as a circulator.

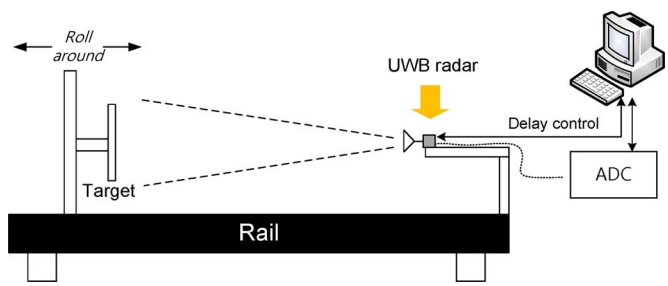

Fig. 8. Measurement setup for the UWB radar TRX.

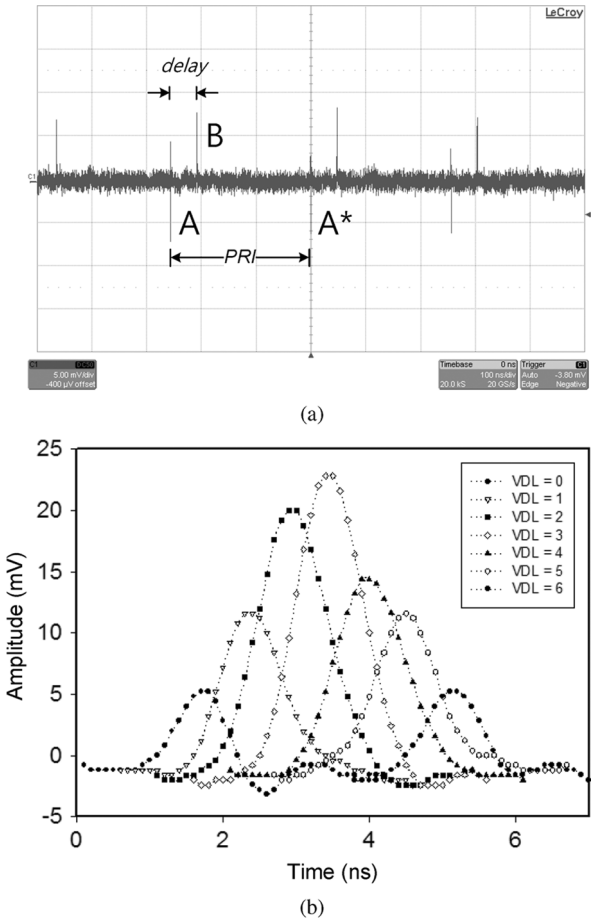

Fig. 9. (a) Measured output pulse train of the receiver. A is the correlation output of a TX pulse and its leakage signal. B is the correlation output of an RX pulse and a delayed-local pulse. (b) Enlarged waveform of the correlation output of a RX pulse and a delayed-local pulse with varying VDL. Seven steps of delays are used to scan a period of carrier frequency.

about seven steps are required to scan a period of the carrier frequency. The carrier frequency is 26 GHz and the delay step of the VDL is about 5.5 ps.

The measured output waveform is shown in Fig. 10 when the target is 1.03 m away from the radar. The envelope of the output signal is due to convolution of the pulse shape, and the fluctuations in the envelope are due to the phase. To find the peak amplitude, 22 coarse and four fine delays are needed. The measured delay is 22×500 ps $+ 4 \times 5.5$ ps $= 11.02$ ns, which is translated to 1.03 m with calibration.

In Fig. 11, a magnified graph of the correlation output pulse train is shown when the target is detected. The target is moved from 500 to 505 mm by 1-mm steps. The figure shows that the UWB radar can detect 1-mm movement of the target.

The distance between TRX and the target is measured in Fig. 12. The target is moved from 0.2 to 8.0 m, and the target range is detected in two ways: peak detection (max) finds the delay of the maximum output value and cross-correlation detection (corr) finds the delay of the maximum cross-correlation output value of a pre-defined template and incoming measured data. The measured maximum errors of the peak and cross-correlation detection are 11.5 and 4 mm, respectively. The measured maximum standard deviations of the peak and cross-correlation detection are 9.9 and 2.8 mm, respectively. All results are measured ten times, and a laser distance meter (Leica Disto plus) is used for comparison.

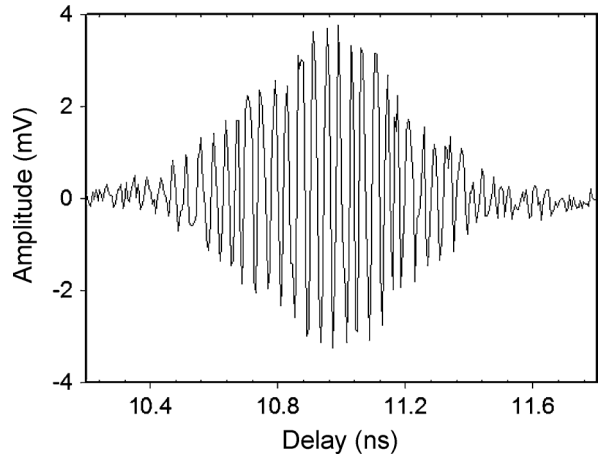

Fig. 10. Measured output waveform of the UWB radar TRX (Distance $=$ 1.03 m).

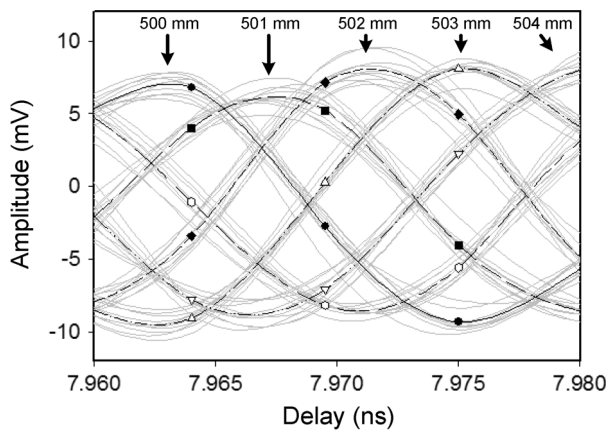

Fig. 11. Measured distance accuracy. The target is moved from 500 to 505 mm by 1-mm step. Every result is measured ten times and averaged.

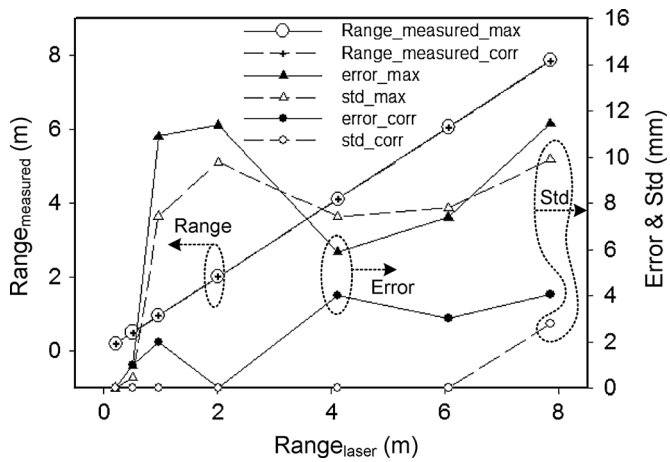

Fig. 12. Measured range between the TRX and a target, and its error and standard deviation. Two methods are applied for range detection: peak detection (max) and cross-correlation detection (corr).

The measured output pulse trains of TRX 1 and 2, which are from self-correlation of the leakage signals, are shown in

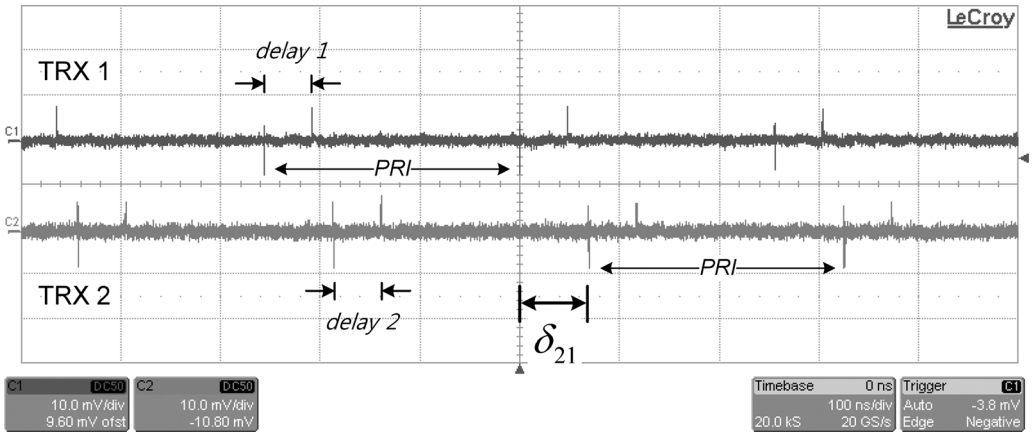

Fig. 13. Measured output pulse trains of the TRX 1 and 2. Pulses are from the self-correlated leakage signals.

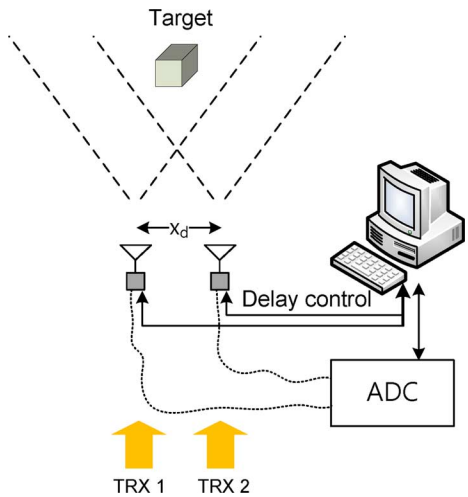

Fig. 14. Measurement setup for the synchronization test and the MIMO operation.

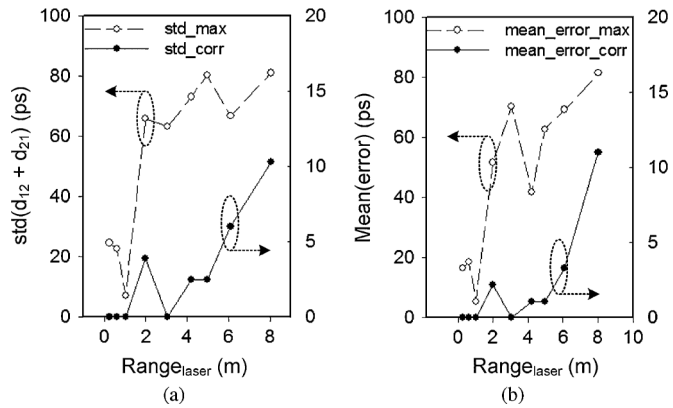

Fig. 15. Measured results of the synchronization test. (a) Standard deviation of the measured $d_{12}+d_{21}$. (b) Mean error between $d_{12}+d_{21}$ and $2t_d+T_P$, which are measured by the UWB radar TRXs and the laser distance meter, respectively. Each of the results is measured with both peak and cross-correlation detection methods.

Fig. 13. The output pulses indicate the timings of transmitting a pulse and correlating a delayed local pulse and a received signal. Delay 1 and delay 2 are the controlled delays of TRX 1 and 2, respectively. The asynchronous time difference δ_{21} can be estimated from the measured output pulse trains.

To verify the accuracy of the wireless cooperative synchronization, the measured delays of swapped signals are compared with the measured traveling times from the laser distance meter due to the difficulties of measuring δ_{21}. The accuracy of δ_{21} from $d_{12}-d_{21}$ can be verified through $d_{12}+d_{21}$. TRX 1 and TRX 2 are placed as shown in Fig. 14 and the space between the TRXs, X_d, is set close to 0 m to compare these results correctly by making the same lines of sight of the TRXs and the laser distance meter. From (12)–(15), $d_{12}+d_{21}$ can be deduced in each case for comparison with the measured traveling times from the laser distance meter. For example, $d_{12}+d_{21}=2t_d+T_P$ is obtained from (14), and $d_{12}+d_{21}$ and $2t_d+T_P$ are compared. The delays d_{12} and d_{21} are from the TRXs, and t_d is from the laser distance meter. In Fig. 15, the standard deviation of $d_{12}+d_{21}$ and the mean error between $d_{12}+d_{21}$ and $2t_d+T_P$ are shown when a target is moved from 0.25 to 8.0 m. All results are analyzed from ten iterations of the measurement. The maximum standard deviation is 81 and 10 ps, and the maximum mean error is 81 and 11 ps with the peak and cross-correlation detection methods, respectively.

B. MIMO Operation

MIMO operation is verified by using a pair of UWB radar TRXs. Two TRXs are located with $X_d = 0.30$ m, as seen in Fig. 14.

Output waveforms of TRX 1 and 2 are shown in Fig. 16. Since the MIMO operation gives 2-D range information, the locations of TRXs and targets should be specified in a rectangular coordinate system. TRX 1 and 2 are located at $(-0.15$ m, 0) and (0.15 m, 0), respectively, and the target is located at (0, 1.04 m).

Each TRX can distinguish whether the output pulses are from it (R_{11} and R_{22}) or the other TRXs (T_{12} and T_{21}) by modulation schemes (BPSK and PPM), but in this case, the asynchronous time difference is large enough to display them separately. The delays, d_{11} and d_{22}, indicate the round-trip time of a pulse signal from the target to TRX 1 and 2, respectively. However, d_{12} and d_{21} cannot make correct estimation of the trip time of a pulse signal from TRX 2 through the target to TRX 1, and vice versa, because of δ_{21}. Equations (16)–(19) are proposed to solve this problem. From the measured delays of d_{11} and d_{22}, 1.055- and

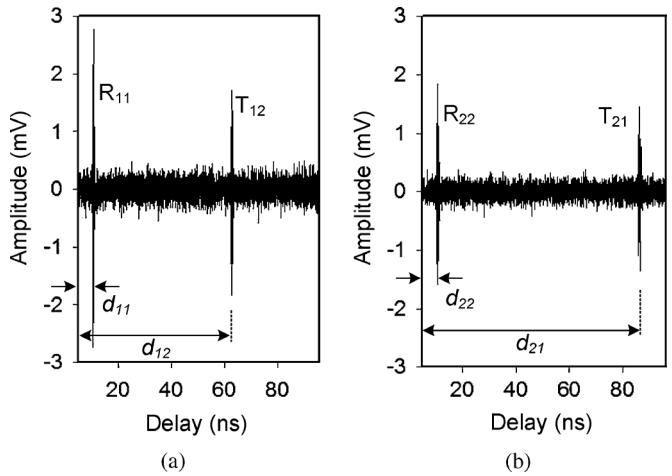

Fig. 16. (a) Measured output waveform of TRX 1. R_{11} and T_{12} are the correlation outputs of the pulses from TRX 1 and TRX 2 with the time-delayed local pulse of TRX 1, respectively. (b) Measured output waveform of TRX 2. R_{22} and T_{21} are the correlation outputs of the pulses from TRX 2 and TRX 1 with the time-delayed local pulse of TRX 2, respectively.

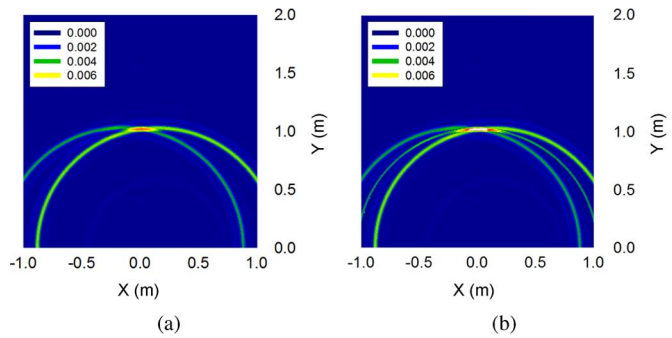

Fig. 17. Measured 2-D image when the target is at (0 m, 1.04 m). (a) Typical distributed radars: two circles, from the d_{11} and d_{22}, are overlapped. (b) MIMO radar: an ellipse, from d_{12} and d_{21}, is added.

1.050-m distances are acquired, and the reference measurement with a laser distance meter gives values of 1.054 and 1.053 m, respectively. Since the first condition for the ambiguities shows that $d_{11} + d_{22} < d_{12} + d_{21}$ from Fig. 16, $d_{12} + d_{21}$ and $2t_d + T_P$ from (14) are selected and they are compared to examine whether d_{12} and d_{21} are valid. These two equations show 10-ps error.

The range information from the multiple TRXs that are spread in space can make a 2-D image using trilateration. From the locations of the TRXs and the measured distances, intersection points of circles can be made, and the points indicate the location of the target. A measured 2-D image is shown in Fig. 17. The intensity of the target location is high when the range circles from both TRXs overlap. In a typical distributed radar system, the locations are acquired by two range circles, but in a MIMO radar, an additional range ellipse, which is gained through synchronization, is also used for MIMO operation.

Spatial diversity is obtained from the spatially spread radar TRXs, as described in Fig. 18. A metal plate is used as a target, and the RCS of the plate is changed by rotating it. If the metal plate and the radar TRXs face each other (0°), the location of

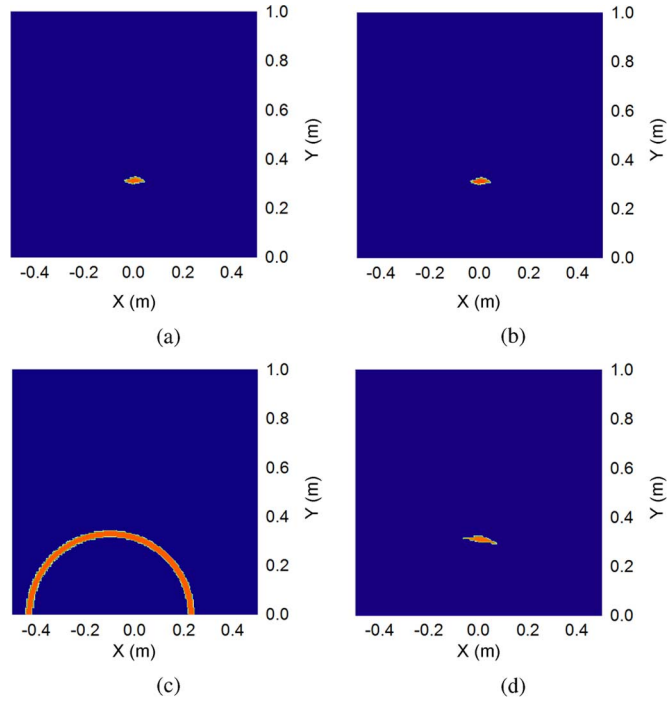

Fig. 18. Spatial diversity is measured with a target that varies the direction of the plane with respect to the radar direction. (a) 0° with typical distributed radars. (b) 0° with the MIMO radar. (c) 10° with typical distributed radars. (d) 10° with the MIMO radar.

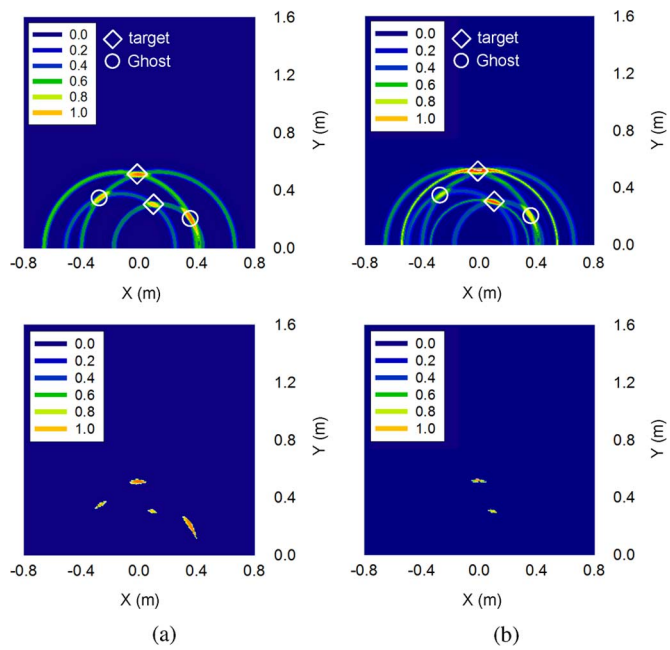

Fig. 19. Two targets are measured to show the ghost problem. (a) Ghosts with the typical distributed radars. (b) Ghosts are disappeared with the MIMO radar.

the target is acquired in both typical distributed radars and the MIMO radar. However, if the metal plate is rotated clockwise (10°), the radar TRX in the right-hand side receives a very weak echo signal, and the typical distributed radars cannot show the target location. The MIMO radar has spatial diversity from the MIMO operation based on the synchronization, and the target location can be identified.

The conventional trilateration methods have a ghost problem when there are multiple targets [5]–[7], [22]. The radar TRXs indicate locations of targets that do not exist at that locations in reality. The ghost problem is shown in Fig. 19. The targets are located at (0 m, 0.55 m) and (0.1 m, 0.32 m). The typical distributed radars show four crossings for target detections including ghosts. However, the MIMO radar filters the ghosts out with the additional range ellipses from the MIMO operation.

VI. Conclusion

A wireless cooperative synchronization method and a coherent fine delay-based radar TRX have been proposed for MIMO operation of radar arrays with widely separated antennas. We have shown the operation of the radar TRX with a coherent pulse generator, a fine delay-based correlator, and a digitally controlled delay. The wireless cooperative synchronization method has been demonstrated using the radar TRXs. Distance measurement results of the TRX show that the maximum mean error is 4 mm for the target in a range of 0.2–8.0 m. Synchronization measurements of two radar TRXs show that the maximum mean error of the measured asynchronous time difference is 11 ps. 2-D image measurements show that the spatial diversity provides tolerance to RCS variations and avoids ghost problems of multiple targets.

Acknowledgment

The authors would like to thank the Integrated Circuit (IC) Design Education Center (IDEC) for their support in computer-aided design (CAD) tools.

References

[1] R. Feger, C. Wagner, S. Schuster, S. Scheiblhofer, H. Jager, and A. Stelzer, "A 77-GHz FMCW MIMO radar based on an SiGe single-chip transceiver," *IEEE Trans. Microw. Theory Techn.*, vol. 57, no. 5, pp. 1020–1035, May 2009.

[2] H. Krishnaswamy and H. Hashemi, "A fully integrated 24 GHz 4-channel phased-array transceiver in 0.13 μm CMOS based on a variable-phase ring oscillator and PLL architecture," in *IEEE Int. Solid-State Circuits Conf. Tech. Dig.*, 2007, pp. 124–126.

[3] A. Babakhani, X. Guan, A. Komijani, A. Natarajan, and A. Hajimiri, "A 77-GHz phased-array transceiver with on-chip antennas in silicon: Receiver and antennas," *IEEE J. Solid-State Circuits*, vol. 41, no. 12, pp. 2795–2806, Dec. 2006.

[4] C.-Y. Kim, D.-W. Kang, and G. M. Rebeiz, "A 44–46-GHz 16-element SiGe BiCMOS high-linearity transmit/receive phased array," *IEEE Trans. Microw. Theory Techn.*, vol. 60, no. 3, pp. 730–742, Mar. 2012.

[5] F. Fölster, H. Rohling, and U. Lubbert, "An automotive radar network based on 77 GHz FMCW sensors," in *IEEE Radar Conf.*, 2005, pp. 3–8.

[6] F. Fölster and H. Rohling, "Data association and tracking for automotive radar networks," *IEEE Trans. Intell. Transport. Syst.*, vol. 6, no. 4, pp. 370–377, Dec. 2005.

[7] J. Kleef, J. Bergmans, L. Kester, and F. Groen, "Multiple-hypothesis trilateration and tracking with distributed radars," in *9th Int. Inform. Fusion Conf.*, Jul. 2006, pp. 1–7.

[8] J. Li and P. Stoica, "MIMO radar with colocated antennas," *IEEE Signal Process. Mag.*, vol. 24, no. 5, pp. 106–114, Sep. 2007.

[9] A. M. Haimovich, R. S. Blum, and J. L. J. Cimini, "MIMO radar with widely separated antennas," *IEEE Signal Process. Mag.*, vol. 25, no. 1, pp. 116–129, Jan. 2008.

[10] A. Stelzer, M. Jahn, and S. Scheiblhofer, "Precise distance measurement with cooperative FMCW radar units," in *IEEE Radio Wireless Symp.*, Jan. 2008, pp. 771–774.

[11] S. Roehr, P. Gulden, and M. Vossiek, "Precise distance and velocity measurement for real time locating in multipath environments secondary radar approach," *IEEE Trans. Microw. Theory Techn.*, vol. 56, no. 10, pp. 2329–2339, Oct. 2008.

[12] R. Feger, C. Pfeffer, W. Scheiblhofer, C. M. Schmid, M. J. Lang, and A. Stelzer, "A 77-GHz cooperative secondary radar system for local positioning applications," in *IEEE MTT-S Int. Microw. Symp. Dig.*, 2012, pp. 8–10.

[13] I. Gresham, A. Jenkins, R. Egri, C. Eswarappa, N. Kinayman, N. Jain, R. Anderson, F. Kolak, R. Wohlert, S. Bawell, J. Bennett, and J.-P. Lanteri, "Ultra-wideband radar sensors for short-range vehicular applications," *IEEE Trans. Microw. Theory Techn.*, vol. 52, no. 9, pp. 2105–2122, Sep. 2004.

[14] J. Yang, G. Pyo, C. Kim, and S. Hong, "A 24-GHz CMOS UWB radar transmitter with compressed pulses," *IEEE Trans. Microw. Theory Techn.*, vol. 60, no. 4, pp. 1117–1125, Apr. 2012.

[15] V. Jain, F. Tzeng, L. Zhou, and P. Heydari, "A single-chip dual-band 22-to-29 GHz/77-to-81 GHz BiCMOS transceiver for automotive radars," in *IEEE Int. Solid-State Circuits Conf. Tech. Dig.*, 2009, pp. 308–310.

[16] E. Ragonese, A. Scuderi, V. Giammello, E. Messina, and G. Palmisano, "A fully integrated 24 GHz UWB radar sensor for automotive applications," in *IEEE Int. Solid-State Circuits Conf. Tech. Dig.*, 2009, pp. 306–308.

[17] R. S. Blum and A. M. Haimovich, "Non-coherent MIMO radar for target estimation: More antennas means better performance," in *43rd Annu. Inform. Sci. Syst. Conf.*, Mar. 2009, pp. 108–113.

[18] S. Lee, S. Kong, C.-Y. Kim, and S. Hong, "A low-power K-band CMOS UWB radar transceiver IC for short range detection," in *IEEE Radio Freq. Integr. Circuits Symp.*, Jun. 2012, pp. 503–506.

[19] M. Skolnik, *Introduction to Radar Systems*. New York, NY, USA: McGraw-Hill, 2002.

[20] S. Lee, C.-Y. Kim, and S. Hong, "K-band CMOS UWB radar transmitter with a biphase modulating pulsed oscillator," *IEEE Trans. Microw. Theory Techn.*, vol. 60, no. 5, pp. 1405–1412, May 2012.

[21] S. Kong, C.-Y. Kim, and S. Hong, "A K-band UWB low noise CMOS mixer with bleeding path GM-boosting technique," *IEEE Trans. Circuits Syst. II, Exp. Briefs*, vol. 60, no. 3, pp. 117–121, Mar. 2013.

[22] Y.-Z. Hu, T.-J. Li, and Z.-O. Zhou, "Use of the location inverse solution to reduce ghost images," *EURASIP J. Adv. Signal Process.*, vol. 2010, pp. 1–8, 2010.

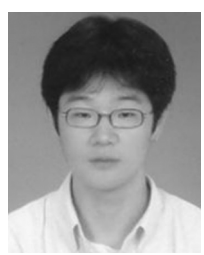

Sunwoo Kong (S'07) received the B.S. and M.S. degrees in electrical engineering from the Korea Advanced Institute of Science and Technology (KAIST), Daejeon, Korea, in 2007 and 2009, respectively, and is currently working toward the Ph.D. degree at KAIST.

His research interests include UWB high-frequency integrated circuits and radar systems.

Sungeun Lee (S'07) received the B.S. and M.S. degrees in electronics engineering from the Korea Advanced Institute of Science and Technology (KAIST), Daejeon, Korea, in 2007 and 2009, respectively, and is currently working toward the Ph.D. degree at KAIST.

His research interests include CMOS RF integrated circuits (RFICs) and systems for short-range radar.

Choul-Young Kim (S'04–A'07) received the B.S. degree in electrical engineering from Chungnam National University (CNU), Daejeon, Korea, in 2002, and the M.S. and Ph.D. degrees in electrical engineering from the Korea Advanced Institute of Science and Technology (KAIST), Daejeon, Korea, in 2004 and 2008, respectively.

From March 2009 to February 2011, he was a Postdoctoral Research Fellow with the Department of Electrical and Computer Engineering, University of California at San Diego (UCSD), La Jolla, CA, USA. He is currently an Assistant Professor of electronics engineering with Chungnam National University, Daejeon, Korea. His research interests include millimeter-wave integrated circuits and systems for short-range radar and phased-array antenna applications.

Songcheol Hong (S'87–M'88) received the B.S. and M.S. degrees in electronics from Seoul National University, Seoul, Korea, in 1982 and 1984, respectively, and the Ph.D. degree in electrical engineering from The University of Michigan at Ann Arbor, Ann Arbor, MI, USA, in 1989.

In May 1989, he joined the faculty of the Department of Electrical Engineering and Computer Science, Korea Advanced Institute of Science and Technology (KAIST), Daejeon, Korea. In 1997, he held short visiting professorships with Stanford University, Palo Alto, CA, USA, and Samsung Microwave Semiconductor, Suwon, Korea. His research interests are microwave integrated circuits and systems including power amplifiers (PAs) for mobile communications, miniaturized radar, millimeter-wave frequency synthesizers, and novel semiconductor devices.